RSC Advances

PAPER

View Article Online
View Journal | View Issue

Cite this: *RSC Adv.*, 2019, **9**, 25919

Triazole-based novel bis Schiff base colorimetric and fluorescent turn-on dual chemosensor for Cu^{2+} and Pb^{2+}: application to living cell imaging and molecular logic gates†

Kalyani Rout, Amit Kumar Manna, Meman Sahu, Jahangir Mondal, Sunil K. Singh and Goutam K. Patra *

Received 6th May 2019
Accepted 9th August 2019

DOI: 10.1039/c9ra03341f

rsc.li/rsc-advances

A triazole-based novel bis Schiff base colorimetric and fluorescent chemosensor (**L**) has been designed, synthesized and characterized by elemental analysis, ^{1}H-NMR, ESI-MS, FTIR spectra and DFT studies. The receptor **L** showed selective and sensitive colorimetric sensing ability for Cu^{2+} and Pb^{2+} ions by changing color from colorless to yellow and light yellow respectively in CH_3OH–tris-buffer (1 : 1, v/v). However, it displayed strong fluorescence enhancement upon the addition of both Cu^{2+} and Pb^{2+} ions, attributed to the blocking of PET. The fluorometric detection limits for Cu^{2+} and Pb^{2+} were found to be 12×10^{-7} M and 9×10^{-7} M and the colorimetric detection limits were 3.7×10^{-6} M and 1.2×10^{-6} M respectively; which are far below the permissible concentration in drinking water determined by WHO. Moreover, it was found that chemosensor **L** worked as a reversible fluorescence probe towards Cu^{2+} and Pb^{2+} ions by the accumulation of S^{2-} and EDTA respectively. Based on the physicochemical and analytical methods like ESI-mass spectrometry, Job plot, FT-IR, ^{1}H-NMR spectra and DFT studies the detection mechanism may be explained as metal coordination, photoinduced electron transfer (PET) as well as an internal charge transfer (ICT) process. The sensor could work in a pH span of 4.0–12.0. The chemosensor **L** shows its application potential in the detection of Cu^{2+} and Pb^{2+} in real samples, living cells and building of molecular logic gate.

Introduction

Simply designed and cost effective chemical sensors have played important roles in monitoring many environmental and biologically relevant species such as heavy metal ions over the past few years. Sensors used for metal ion detection featuring both metal binding property and fluorescence emission subunits are in high demand. Poor selectivity and the fluorescence quenching properties are generally observed in case of fluorescent chemosensors related to small molecules. Although recent progress has been made in this area, there remains a need to develop new tools for the detection of metal ions. The ease of synthesis, high sensitivity, selectivity and low cost are key factors of organic sensors over other recognition methods.

Copper, the third most abundant transition metal ion is an essential trace element for both plants and animals, including humans. Cu^{2+} ions are used in several physiological processes. Copper containing proteins are useful as redox catalysts in biological processes that involve electron transfer reactions and oxidation of various organic substrates.[1,2] It can accumulate in the environment, resulting food and water contamination. According to the World Health Organisation (WHO), the maximum acceptable limit of copper for drinking water is 1 mg L^{-1}.[3] High Cu^{2+} concentration in neuronal cytoplasm can lead to Wilson's disease, Menkes's disease and Alzheimer's disease,[4,5] excessive copper intake results in toxicity and causes irritation of nose and throat resulting in nausea, vomiting, and diarrhea.[6] Cu^{2+} is known to quench emissive states through a variety of different routes, which leads to a turn-off signal.[7–9] For instance, Wang *et al.* reported a new on-off fluorescent and colorimetric chemosensor based on 1,3,4-oxadiazole derivative for the detection of Cu^{2+} ions.[10] Turn-on fluorescent chemosensors are much more beneficial compared to turn-off chemosensors in terms of sensitivity. Only a few Cu(II) based sensors that causes an increase in the fluorescence intensity have been reported.[11] Hence, the design and synthesis of chemosensors with turn-on fluorescence signal for Cu^{2+} are in high interest for researchers in recent years.[12–14] Further, sensors with both colorimetric and turn on fluorescence signal which can respond at extremely low concentration of analyte are in high demand in the analytical and scientific areas because such

Department of Chemistry, Guru Ghasidas Vishwavidyalaya, Bilaspur, CG, India. E-mail: patra29in@yahoo.co.in; Tel: +91 7587312992

† Electronic supplementary information (ESI) available: Fig. S1–S18. See DOI: 10.1039/c9ra03341f

low concentration of analyte(s) can be presently detected by inexpensive instrumentations and synthetically complex molecular systems.

Pb is considered to be the second most toxic heavy metal element and non-degradable in nature. Accumulation of high levels of Pb in children can cause irreversible brain damage and retard mental as well as physical developments. It also causes various health effects, such as anaemia, physical growth impairments, decreased IQ level, memory loss, irritability, muscle paralysis, kidney disorders and mental retardation in the body.[15–17] Despite of these facts, the use of Pb cannot be controlled in modern life because of its wide applications in insulation, coating, electronics, paints and storage batteries. Hence it is highly desirable to develop a more sensitive and selective receptor which can detect Pb^{2+} below the limit recommended by the WHO.[18] There are various techniques to detect Pb^{2+} like atomic absorption spectrometry and inductively coupled plasma mass spectrometry *etc.* The Schiff base turn on Pb^{2+} sensors are scarce in the literature.[19,20]

In continuation to our on-going reach interest[21,22] herein, we have synthesized a triazole-appended Schiff base chemosensor **L**, which showed fluorescence enhancement upon interaction with both Pb^{2+} and Cu^{2+} and change in color in CH_3OH–tris buffer (10 mM, pH 7.2) medium (1 : 1). The selected strategy behind the designing of this chemosensor **L** is mainly based on three facts. Firstly, the "N"-rich triazole moiety along with >C=N functionality may effectively participate for metal coordination. Secondly, introduction of strong electron donating group (–OH, –OMe) is necessary to construct ICT based donor–π conjugation–acceptor (D–π–A) channel, as the acceptor site (>C=N) is connected to electron rich triazole, which somewhat lowers its electron accepting character. Moreover bis Schiff base has been selected, as the presence of two (D–π–A) channels, the affinity towards selected metal may increase and make the detection limit lower. To the best of our knowledge, this is the first time, where 1,2,4-triazole-Schiff base (**L**) is being employed as the colorimetric and fluorescent turn on probe for Cu^{2+} and Pb^{2+}.

Experimental

General information

All of the materials used for synthesis were obtained from Sigma Aldrich and used without further purification. Solvents used for the experimental purpose were of analytical grade. Freshly de-ionized water was used throughout the experiment. Nitrate salts of respective cations were used for the preparation of the stock solutions. Microanalyses were carried out using a PerkinElmer 2400II elemental analyzer. The melting point was determined by an Electrothermal IA9000 series digital melting point apparatus and is uncorrected. Fourier transform infrared (FT-IR) and solution electronic spectra were recorded on Nicolet Magna-IR (Series II). ^{1}H-NMR spectra were recorded on a Bruker DRX spectrometer operating at 300 MHz in DMSO-d_6 and chemical shift were recorded in ppm relative to TMS. Solution conductivity was measured by a Systronics (India) direct reading conductivity meter. UV-visible spectra were recorded on a Shimadzu UV 1800 spectrophotometer using a 10 mm path length quartz cuvette with the wavelength in the range of 200–800 nm. The emission spectra were recorded on a PerkinElmer LS-55 Fluorescence Spectrometer. Mass spectra were recorded on a Waters mass spectrometer using mixed solvent methanol and triple distilled water which was equipped with an ESI source. The pH measurements carried out using a digital pH meter (Merck). Stock solution of Cu^{2+} was prepared by dissolving $Cu(NO_3)_2$ (3.31 mg, 0.01 mM) in triple distilled water (10 mL). Similarly 0.01 mM stock solution of Pb^{2+} was prepared by mixing 3.31 mg of $Pb(NO_3)_2$ in 10 mL of triple distilled water. A stock solution of **L** (1×10^{-3} M) was prepared by dissolving 4.27 mg in 10 mL of CH_3OH–tris-buffer (1 : 1, v/v). The quantum yields were measured against a standard quinine sulphate solution in 0.1 N H_2SO_4 ($\varphi = 0.54$).

Synthesis and characterization of the chemosensor L

The synthetic procedure of **L** has been illustrated in Scheme 1. 3,5-Diamino-1,2,4-triazole (0.099 g, 1 mmol) was dissolved in 15 mL of anhydrous methanol. To this solution 20 mL methanolic solution of syringaldehyde (0.364 g, 2 mmol) was added dropwise with constant stirring. The reaction mixture was refluxed for 6 h at 70 °C, maintaining dry condition in presence of catalytic amount of glacial acetic acid. A yellowish solid precipitated out, was filtered and washed several times with *n*-hexane and then re-crystallized from methanol and dried in vacuum. Yield, 0.367 g (86%); mp above 250 °C. FT-IR: (KBr, cm^{-1}): 3846 (s-OH), 3736 (s, –NH), 3136 (w, Ar. C–H), 1696 (sb) (C=N of triazole and imine), 1524 (s), 1275 (w), 1135 (w), 923 (w), 868 (w), 839 (w), 764 (m), 751 (s), (Fig. S1†). ^{1}H-NMR: (DMSO, δ ppm, TMS): 9.78 (1H, –NH); 9.13 (s, 2H, –OH); 8.88 (s, 2H, –CH=N); 7.32 (s, 2H, -Ph), 7.21 (s, 2H, –Ph) and 3.85 (s, 12H, $-OCH_3$) (Fig. S2†). ^{13}C-NMR (DMSO, δ ppm, TMS): δ 192.41, 148.42, 142.34, 127.51, 129.96, 107.39, 127.34, 106.71, 56.43 (Fig. S3†). ESI-MS: m/z [M + H$^+$], 428.40 (100%) (Fig. S4†). Anal. calc. for $C_{20}H_{21}N_5O_6$: C, 56.20; H, 4.95; N, 16.39%. Found C, 56.12; H, 4.99; N, 16.43%.

Synthesis and characterization of the copper complex of L (1)

A methanol solution (10 mL) of $Cu(NO_3)_2 \cdot 8H_2O$ (0.165 g, 0.5 mmol) was added dropwise with stirring, to a solution of **L** (0.213 g, 0.5 mmol) in methanol (20 mL). The mixture was stirred for additional 3 h and then the yellow precipitate was collected by filtration, washed with methanol and hexane. Yield, 0.170 g (65%). FTIR/cm^{-1} (KBr): 3095 (s, aromatic CH– str), 1678 (vs, C=N), 1586 (m), 1443 (m), 1388 (m), 1217 (m), 1147 (s), 991 (s), 894 (m), 755 (s), 692 (s) (Fig. S5†). EI-MS: m/z 525.98 (**L** + Cu^{2+} + $2H_2O$) (Fig. S6†). UV-vis λ_{max}/nm (CH_3CN): 460 (22 700) (Fig. S7†). Emission spectra; λ_{max}/nm (CH_3CN): 413 (Fig. S8†). Λ_M/Ω^{-1} cm^{-2} mol^{-1} (CH_3OH): 13 (non-electrolyte). Anal. calc. for $C_{20}H_{24}N_5O_8Cu$: C, 45.67; H, 4.60; N, 13.31%. Found C, 45.53; H, 4.67; N, 13.38%.

Synthesis and characterization of the lead complex of L (2)

Similar method like synthetic procedure of **1** was adopted for the synthesis of the Pb complex, **2**. $Pb(NO_3)_2$ (0.165 g, 0.5 mmol) was used in place of $Cu(NO_3)_2 \cdot 8H_2O$. Light yellow precipitate

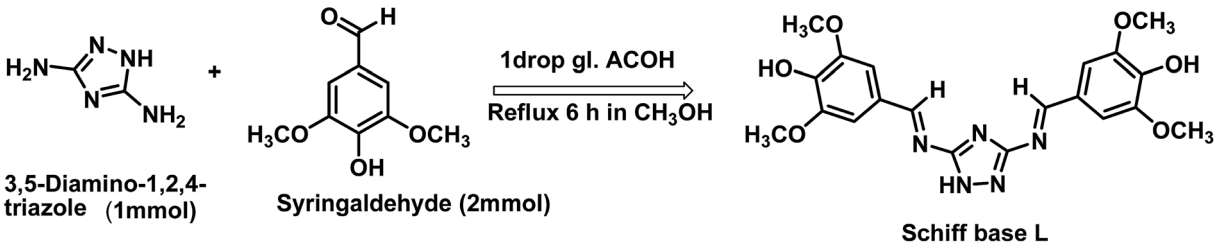

Scheme 1 Synthetic procedure of the probe L.

was collected by filtration. Yield, 0.132 g (46%). FTIR/cm^{-1} (KBr): 3738 (–OH), 2353 (m), 1677 (s, C=N), 1560 (s), 1498 (s), 1418 (s), 1299 (m), 1115 (m), 834 (s), 742 (s), 669 (s) (Fig. S9†). EI-MS: $m/z = 913.87$ (**L** + $2Pb^{2+}$ + $4H_2O$) (Fig. S10†). UV-vis λ_{max}/nm (CH_3CN): 406 (sh), 400. (Fig. S7†). Emission spectra; λ_{max}/nm (CH_3CN): 442 (Fig. S8†). Λ_M/Ω^{-1} cm^{-2} mol^{-1} (CH_3OH): 210 (1 : 2 electrolyte). Anal. calc. for $C_{20}H_{29}N_9O_{22}Pb_2$: C, 20.67; H, 2.52; N, 10.85%. Found C, 20.49.12; H, 2.61; N, 10.76%.

Photophysical studies

The chemosensor **L** (4.27 mg, 0.01 mmol) was dissolved in 10 mL methanol to make the solution 10^{-3} M and 30 μL of this solution was diluted to 3 mL with methanol–tris buffer mixture (1 : 1 v/v) to make a final concentration of 10 μM. The guest cations solution were prepared separately using their nitrate salts in the order of 10 mM, with triple distilled water and further diluted to their desired concentration. After mixing **L** with each of the metal ions for a few seconds, UV-vis and fluorescence spectra were obtained at room temperature.

Job's plot measurements

For determination of stoichiometry between **L** and each metal ion Job's plot analyses were used. A methanol tris buffer (1 : 1) solutions containing **L** (10 μM) and aqueous solution of $Pb(NO_3)_2$ and $Cu(NO_3)_2$ (10 μM each) were prepared separately. Then changing the mole ratio of **L** from 0.1 to 0.9 in such a manner that the sum of the total volume of metal ion and **L** remained constant (2 mL). All the solutions were diluted to 3 mL. After shaking them for a minute, fluorescence spectra were obtained at room temperature.

Competition with other metal ions

To determine the possible interference from other metal ions and selective binding affinity of chemo sensor **L** towards Cu^{2+} and Pb^{2+}, fluorescence spectra were taken in presence of other analytes. Chemosensor **L** (4.27 mg, 0.01 mmol) was dissolved in the methanol–tris buffer (1 : 1) solvent mixture (10 mL) and 30 μL of it was diluted to 3 mL to make a final concentration of 10 μM. $M(NO_3)_2$ (0.1 mmol) (where, M = Cu^{2+} and Pb^{2+}) were dissolved in 10 mL of triple distilled water (each). 30 μL of each metal solution (10 mM, Al^{3+}, Hg^{2+}, Co^{2+}, Ni^{2+}, Zn^{2+}, Ca^{2+}, Mn^{2+}, Cd^{2+}, Cr^{3+}, Mg^{2+}, Fe^{3+} and Ag^{+}) was taken and added to 3 mL of the solution of receptor **L** (10 μM) to give 10 equiv. of metal ions. Then, 30 μL of metal solution (10 mM) (where, M = Cu^{2+}, and Pb^{2+}) were added to the mixed solution of each metal ion and **L** to make 10 equiv. After mixing them for seconds, fluorescence spectra were obtained at room temperature.

pH effect test

The charge distribution of the free receptor **L** and its metal complex solutions were affected with variation of pH which is responsible for difference absorption behaviour of solution. For preparing solutions of different pH values ranging from 1 to 12, HCl and NaOH solutions were used. To stabilise these solutions of varied pH values, buffer solutions were prepared in water: pH 1–2, KCl/HCl; pH 3–4, CH_3COOH/KOH; pH 5–7, HEPES/HCl; pH 8–9, tris/KOH; pH 10–11, $NaHCO_3$/KOH; pH 12, NaCl/KOH and then added to the relevant solution.[23] After a solution with the desired pH was achieved, receptor **L** (4.27 mg, 0.01 mmol) was dissolved in methanol (10 mL), and then 30 μL of this solution (1 mM) was diluted to 3 mL with the abovementioned buffers to make the final concentration of 10 μM. $Pb(NO_3)_2$ (33.1 mg, 0.1 mmol). 30 μL of the Pb^{2+} solution (10 mM) was transferred to each receptor solution (10 μM) prepared above. After few seconds of mixing, fluorescence spectra were obtained at room temperature. The same procedures were followed for Cu^{2+}.

Computational details

The GAUSSIAN-09 Revision C.01 program package was used for all calculations.[24] The gas phase geometries of the chemosensor **L** was fully optimized without any symmetry restrictions in singlet ground state with the gradient-corrected DFT level coupled with the hybrid exchange–correlation functional that uses Coulomb-attenuating method B3LYP.[25] Basis set 6-31++G was found to be suitable for the whole molecule. LanL2DZ basis sets were implemented for the geometry optimization of **L** + Cu^{2+} and **L** + Pb^{2+} complexes.

Methods for cell imaging

HeLa cells were cultured in Dulbecco's modified Eagle's medium (DMEM) supplemented with 10% fetal bovine serum (FBS) at 37 °C for 2 h. Cells were placed on 18 mm glass cover slips and allowed to adhere for 24 h. The cells cultured in DMEM were treated with 10 μM solutions of chemosensor **L** dissolved in 10% DMSO and incubated at 37 °C for 2 h. The treated cells were washed with PBS three times to remove **L**. DMEM (2 mL) was added to the cell culture, which was then treated with a 10 μM solution of $Cu(NO_3)_2$. The samples were

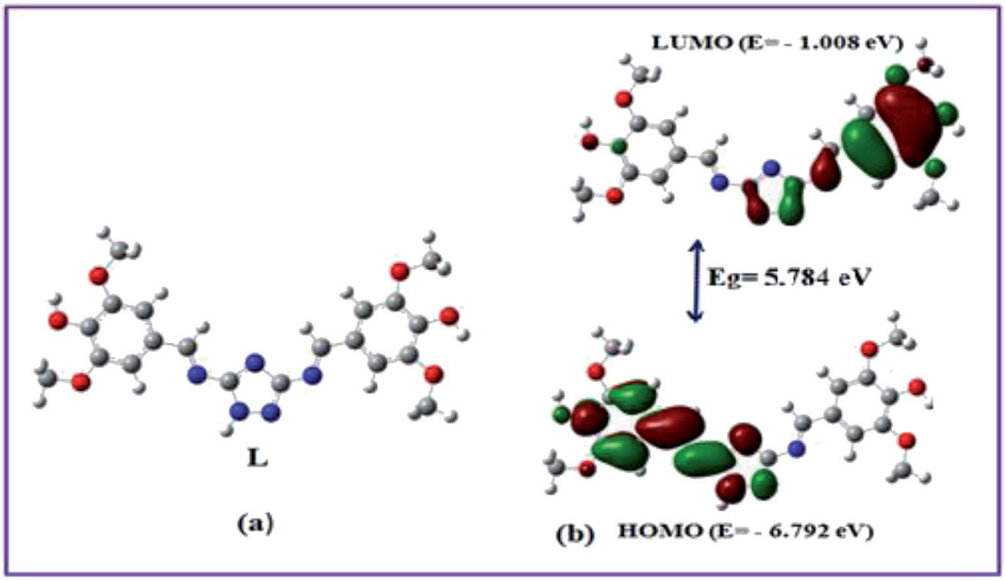

Fig. 1 Optimized geometry, frontier molecular orbitals and HOMO–LUMO energy gap of the probe L.

incubated at 37 °C for 2 h under the same imaging condition. These incubated cells were washed with PBS and mounted onto a glass slide.[26] The fluorescent images of the mounted cells were obtained using a confocal laser scanning microscope with excitation at 450 nm. For Pb^{2+} same procedure was followed.

Result and discussion

Synthesis and structure of L

Ligand **L** was obtained in good yield by the condensation reaction of 3,5-diamino-1,2,4-triazole and syringaldehyde (Scheme 1), and characterized by ^{1}H-NMR, ^{13}C-NMR, FT-IR spectrometer, ESI-mass spectroscopy and elemental analysis.

In order to get the most probable structure of **L**, computations on the chemosensor **L** was performed based on density functional theory (DFT). The geometry optimized structure and a schematic representation of the energy of MOs and contours of selected HOMO and LUMO orbitals of **L** has been shown in Fig. 1. The calculated energy gap between HOMO and LUMO in **L** is 5.784 eV.

UV-vis spectral responses

The electronic absorption spectrum of **L** (10 μM in CH_3OH–tris buffer) exhibits two prominent bands at 330 and 270 nm. The absorption band at 330 nm was attributed to n–π* transitions, while another band at 270 nm was assigned to the π–π* transitions.[27] The cation-binding properties of ligand **L** were evaluated in CH_3OH–tris buffer (1 : 1 v/v) mixture by addition of 3 equiv. of different metal cations such as Al^{3+}, Cu^{2+}, Cd^{2+}, Hg^{2+}, Pb^{2+}, Zn^{2+}, Co^{2+}, Ni^{2+}, Ca^{2+}, Mn^{2+}, Cr^{3+}, Mg^{2+}, Fe^{3+} and Ag^{+}. As shown in Fig. 2, only Cu^{2+} showed a new peak at 460 nm with a color change from colorless to yellow whereas Pb^{2+} displayed a broad peak centered at 400 nm with two shoulders due to larger π-electron delocalization, leading to a colour change from colorless to light yellow. Other cations such as Al^{3+}, Hg^{2+}, Co^{2+}, Ni^{2+}, Zn^{2+}, Ca^{2+}, Mn^{2+}, Cd^{2+}, Cr^{3+}, Mg^{2+}, Fe^{3+} and Ag^{+} showed only some decrease of the absorption band under similar condition.

Upon the addition of 2 equiv. of Cu^{2+} to **L**, the absorption band at 270 and 330 nm gradually decreased and a new absorption band appeared at 460 nm. A clear isosbestic point at 355 nm indicated the formation of only one complex species between **L** and Cu^{2+}. The molar extinction coefficient of the new peak at 460 nm is 7×10^3 M^{-1} cm^{-1}, which is too large to be Cu-based d–d transitions and thus must be metal–ligand transitions. As there are red shifts in the absorption spectra of the Cu^{2+} and Pb^{2+} of the chromophore **L**, there are chances for ligand to metal charge transfer (LMCT). Addition of 3 equiv. of Pb^{2+} solution causes decrease in intensity of the absorption

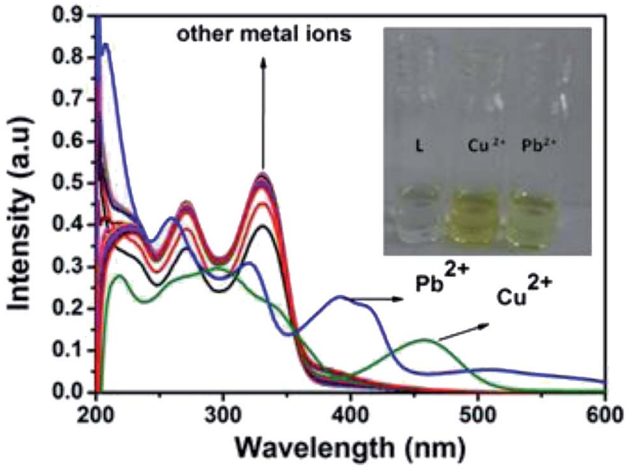

Fig. 2 Absorption spectra of L (10 μM) in presence of 3 equiv. of different metal ions. Inset: colour change of L on addition of 3 equiv. of Pb^{2+} and Cu^{2+}.

band at 330 nm and somewhat blue shifted the band at 270 nm. Abroad new absorption band appears at 400 nm (molar extinction coefficient = 2.6×10^4 M^{-1} cm^{-1}) with an isosbestic point at around 355 nm (Fig. 3). This indicates the formation of a complex between the receptor **L** and Pb^{2+}. The colorimetric detection limits obtained from the titration curves, were found to be 3.7×10^{-6} M and 1.2×10^{-6} M for Cu^{2+} and Pb^{2+} ions respectively (Fig. S11†), which are far below than the WHO guidelines for drinking water. Thus the chemosensor **L** can be applicable as a visual colorimetric probe towards Pb^{2+} and Cu^{2+} ions at the physiological condition.

Effect of metal ions on the emission spectra of probe L

The emission behaviour of **L** was investigated by fluorescence measurements in CH_3OH–tris buffer (10 mM, pH 7.2) medium (1 : 1) with excitation wavelength at 340 nm. In the fluorescence spectra, the free receptor **L** displayed very weak emission at about 440 nm. The fluorescence changes upon addition of a wide range of metal cations including Ag^{+}, Al^{3+}, Mn^{2+}, Fe^{3+}, Ag^{+}, Cu^{2+}, Pb^{2+}, Zn^{2+}, Co^{2+}, Ni^{2+}, Cr^{3+}, Cd^{2+} and Hg^{2+} in CH_3OH–tris buffer are depicted in Fig. 4. Addition of only Pb^{2+} and Cu^{2+} to the solution of **L** induced fluorescence enhancement whereas no significant spectral changes were observed upon addition of the other background metal ions. These results suggest that complexation between **L** and Cu^{2+} and Pb^{2+} ions through intermolecular interaction might be taking place. To further investigate the insight mechanism of complexation, fluorescence titration experiments of **L** in presence of Pb^{2+} and Cu^{2+} were performed independently in the same homogeneous mixture (Fig. 5). Upon stepwise addition of Cu^{2+} ions, the fluorescence intensity of **L** (quantum yield $\varphi = 0.002$) at 440 nm was gradually enhanced by about 15 fold ($\varphi = 0.03$) and blue-shifted to 412 nm. Similarly in case of Pb^{2+} fluorescence intensity at 440 nm was increased almost 17 times ($\varphi = 0.035$) and 5 equiv. of each metal was enough to reach the plateau. The quenching behaviour of **L** can be due to non-radiative photo induced electro transfer (PET) from free 'imine' and triazole moiety to the excited fluorophore, which results in decrease in fluorescence intensity. Also the free imine site behaves as very weak acceptor due to 'N' rich triazole attached to it. After coordination of particular analytes through the imine (>C=N) and triazole moieties, blocking of PET process occurs which enhanced emission property of **L** and strengthen the ICT process. For Cu^{2+} binding, deprotonation of triazole occurs (*vide supra*, in NMR spectra) which decreases accepting character of imine moiety thus small blue shift in emission band is observed.

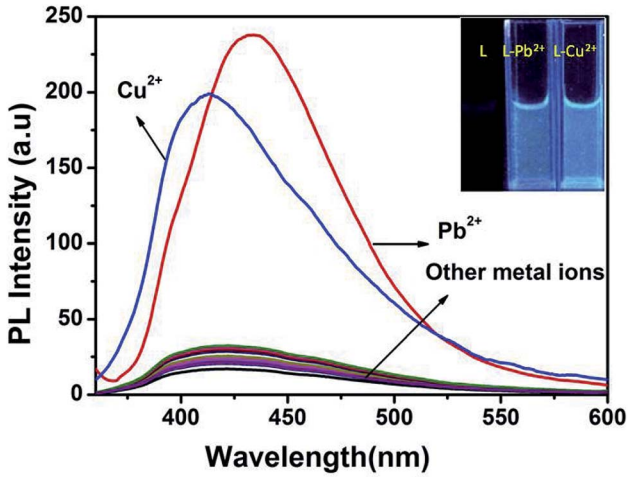

Fig. 4 Fluorescence spectra of L (10 μM) in presence of 5 equiv. different metal ions in CH_3OH–tris buffer (1 : 1) mixture. Inset: colour change of L on addition of 5 equiv. of Pb^{2+} and Cu^{2+} in UV light. Excitation wavelength, 340 nm.

From the titration profile, the fluorometric detection limits for Pb^{2+} and Cu^{2+} ions were calculated to 0.99 μM and 1.24 μM respectively, using the formula $3\sigma/k$ (Fig. S12†). Importantly, the value is much lower than the World Health Organization (WHO) guideline for Cu^{2+} and Pb^{2+} in the drinking water. A careful analysis of the Job's plot indicated 1 : 1 stoichiometric complex between **L** and Cu^{2+} and 1 : 2 complexation stoichiometry between **L** and Pb^{2+} (Fig. S13†), which has further been

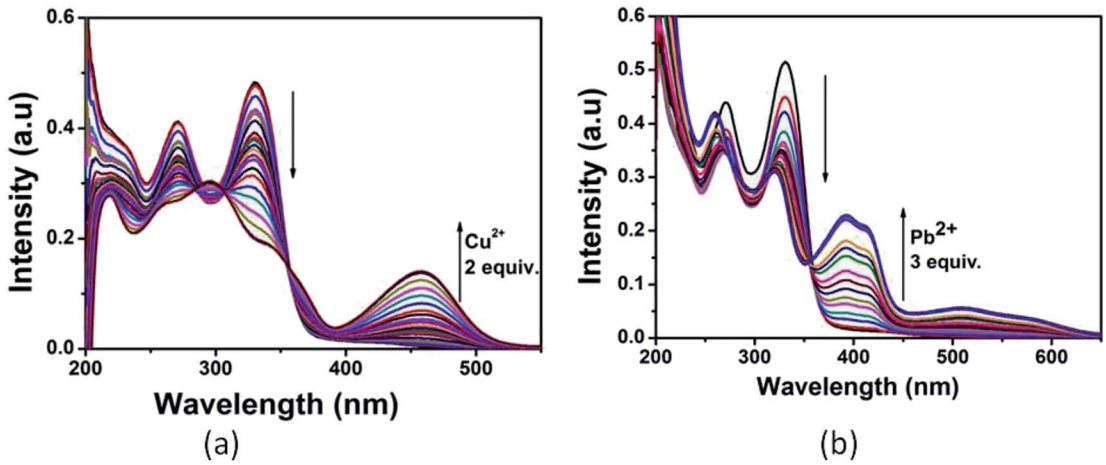

Fig. 3 UV-vis titration of L with (a) Cu^{2+} and (b) Pb^{2+} in CH_3OH–tris buffer.

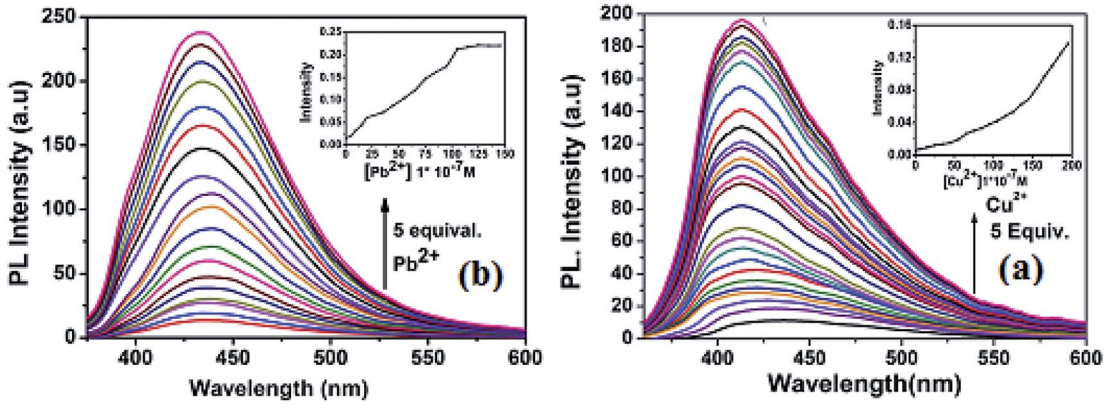

Fig. 5 (a) Fluorescence titration of L (10 μM) with Cu^{2+} (b) fluorescence titration of L with Pb^{2+} in CH_3OH–tris buffer. Excitation wavelength 340 nm.

confirmed by ESI mass spectral analysis. The positive-ion mass spectrum of **1** showed that the peak at $m/z = 525.518$ was assignable to $[(\mathbf{L} + Cu^{2+} + 2H_2O)]$ (Fig. S14†). On magnification, three peaks are observed at $m/z = 525.52$, 526.38 and 527.29 with an intensity ratio of 1 : 0.46 : 0.25. Since for copper the natural abundance of isotope 63, is 70% and that of isotope 65, 30%, the relative intensities of these peaks are calculated as 1 : 0.45 : 0.22. Similarly, the $\mathbf{L} + Pb^{2+}$ provides the molecular ion peak at $m/z = 915.083$, which was assignable to $[(\mathbf{L} + 2Pb^{2+} + 4H_2O)]$ (Fig. S15†). Assuming 1 : 1 and 1 : 2 bonding, the association constants (K_a) of **L** with Cu^{2+} and Pb^{2+} ions were calculated to be 4.7×10^4 M^{-1} and 1.43×10^{11} M^{-2} respectively (Fig. S16†), from the linear fitting of Benesi–Hildebrand method,[28] indicating the strong affinity of Cu^{2+}/Pb^{2+} towards the chemosensor **L**.

To infer the further utility of chemosensor **L** for Cu^{2+} and Pb^{2+} ions, the competitive experiments were conducted by fluorescence measurement of 10 μM **L** in CH_3OH–tris buffer mixture (1 : 1) in the presence of 5 equiv. of Cu^{2+} or Pb^{2+} ion mixed with 5 equiv. of other interfering metal ion (Fig. 6). The emission intensity at 440 nm and 412 nm for Pb^{2+} and Cu^{2+} ion respectively remain almost same, even in presence of 3 fold higher concentrations of background cations. Although emission intensity slightly decreases in presence of Cu^{2+} ion for **L**–Pb^{2+} complex and Co^{2+}, Ni^{2+} ion decreases the fluorescent intensity of **L**–Cu^{2+} complex but it was well assessable. Therefore, chemosensor **L** could be used for real sample analysis as well as biological studies.

In order to investigate the effect of pH on the emission properties of **L**, **L**–Cu^{2+} and **L**–Pb^{2+}, fluorescence spectra were measured in varied pH range of 1–12 (Fig. 7). The decrease in the fluorescence intensity at low pH values can be attributed to the protonation of the imine and triazole coordinating site which reduce efficient metal binding. Overall chemosensor **L** was non-fluorescent within the wide pH range 1–12 whereas for metal complex with increasing pH value ICT become more efficient thus strong fluorescence occurs. Above results revealed

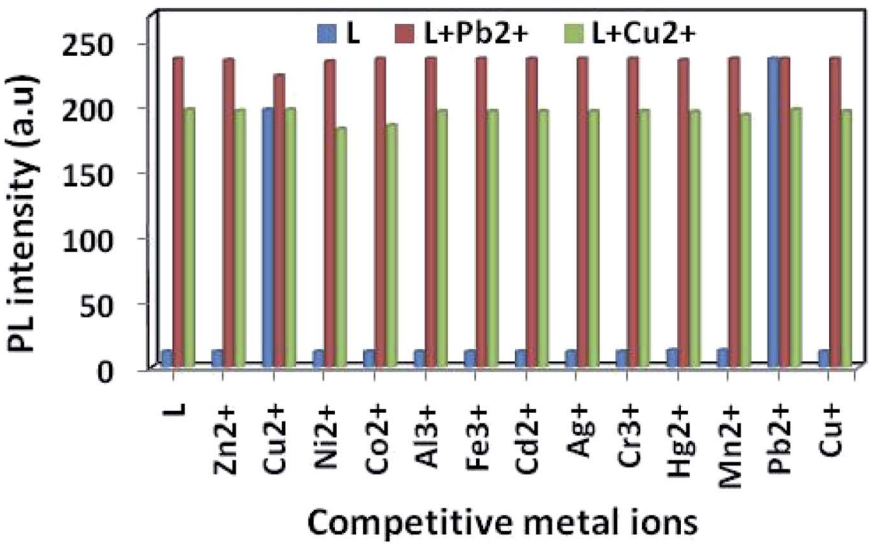

Fig. 6 Fluorescence intensity of L, (10 μM) to 5 equiv. of Cu^{2+}, Pb^{2+} and other cations in CH_3OH–tris buffer (1 : 1, v/v) mixture. Excited wave length 340 nm and emission maxima 412 nm for Cu^{2+} and 440 nm for Pb^{2+}.

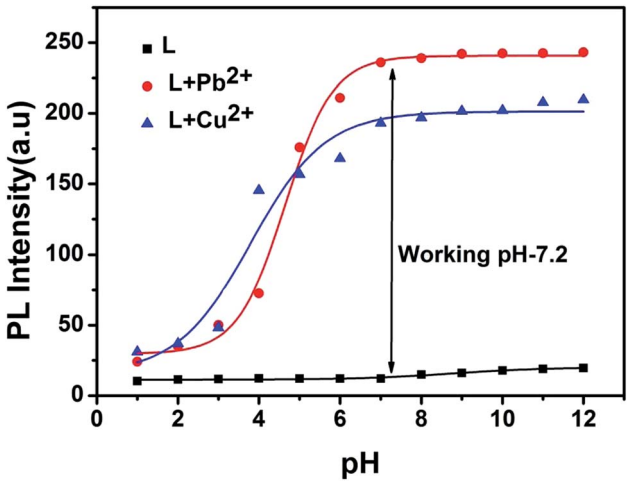

Fig. 7 pH effect of L, L–Cu^{2+} and L–Pb^{2+}.

that **L** can be a good candidate for sensing of both Cu^{2+} and Pb^{2+} in the pH range 4–12.

Fluorescence reversibility experiments for **L** were carried out by alternate addition of 5 equiv. of Cu^{2+} ion and S^{2-} ions (Na_2S) to the 10 μM solution of **L**. As illustrated in Fig. 8, the fluorescence-enhanced emission towards the Cu^{2+} ions was almost completely quenched by simply addition of 5 equiv. of S^{2-} and got the fluorescence spectra of **L**. Approximately 95% of the fluorescence emission could be quenched as a result of the competitive binding phenomenon between **L** and S^{2-} towards Cu^{2+} ions. Consequently, the enhancement in fluorescence spectra of **L** could be achieved after the addition of 5 equiv. of Cu^{2+} ions to the system again. This means that the fluorescence increases by Cu^{2+} ions and quenched by S^{2-} which were repeated for five cycles. In case of Pb^{2+}, with gradual addition of common metal chelator disodium ethylene diamine tetra acetic acid (Na_2EDTA) into the L–Pb^{2+}, the fluorescence at 440 nm quenched as well as original non-fluorescent behavior of **L** was restored. After further addition of 5 μM of Pb^{2+} in this solution of **L**, the fluorescent turn on behaviour of L–Pb^{2+} was regenerated. These observations suggested that fluorescence spectra of the L–Cu^{2+} and L–Pb^{2+} complex can be reversibly restored to that of the uncomplexed ligand **L** by adding S^{2-} and EDTA respectively.

Sensing mechanism of the probe L

The coordination sites of the proposed receptor **L** towards selected guests Cu^{2+} and Pb^{2+} were investigated by ^{1}H-NMR titration experiments in DMSO-d_6 (Fig. 9). The chemical shift at $\delta = 9.7$ ppm due to triazole –NH in free receptor **L** was completely vanished in addition of 1 equiv. Cu^{2+} ion, which confirmed that deprotonation occurred during Cu^{2+} binding. Also the azomethine proton shifted downfield region (from $\delta =$ 8.88 ppm to $\delta = 9.1$ ppm), which confirmed the participation of imine towards complexation. Similarly addition of 2 equiv. Pb^{2+} to **L**, –CH=N proton shifted to 9.25 ppm due to ligand to metal charge transfer (LMCT) process through imine site but there no deprotonation of triazole occurred. The –OH and –OMe protons also shifted towards downfield in both the cases due to chelation induced ICT process. This ^{1}H-NMR behaviour of **L** was consistent even in presence of somewhat higher concentration of both the analytes Cu^{2+} and Pb^{2+}.

To get insight of the sensing mechanism, the Cu and Pb complexes of the probe **L** were isolated as yellow solid on the reaction of receptor–analyte in a 1 : 1 molar ratio in methanol. No single crystals obtained even after several efforts for the Cu–complex (**1**) and Pb–complex (**2**). The FTIR spectra of **L**, **1** and **2** have been shown in Fig. S1, S5 and S9† respectively. In the IR spectra of free ligand **L**, broad band centred around 1696 cm^{-1} may be due to C=N groups (imine moiety of triazole). In **1** and **2** complexes, these bands shifted towards lower wave numbers to 1678 cm^{-1} and 1677 cm^{-1} which suggest that the azomethine groups are involved in the coordination of both the metal ions to the ligand **L**. The band around 1388 cm^{-1} in **2**, may be assigned to the NO_3^- stretching frequency, which is surprisingly absent in the IR spectra of **1**. Further, the peak around 3736 cm^{-1} due to –NH group of ligand **L** became small in L–Pb^{2+} complex and completely vanishes in L–Cu^{2+} complex due to deprotonation. From the elemental analysis, conductance

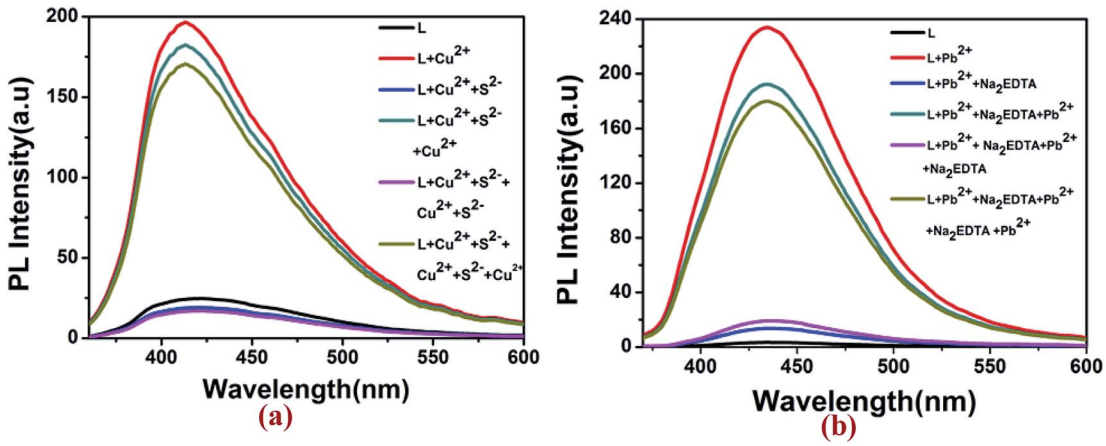

Fig. 8 Reversibility study of (a) L–Cu^{2+} complex with Na_2S and (b) L–Pb^{2+} complex with Na_2EDTA.

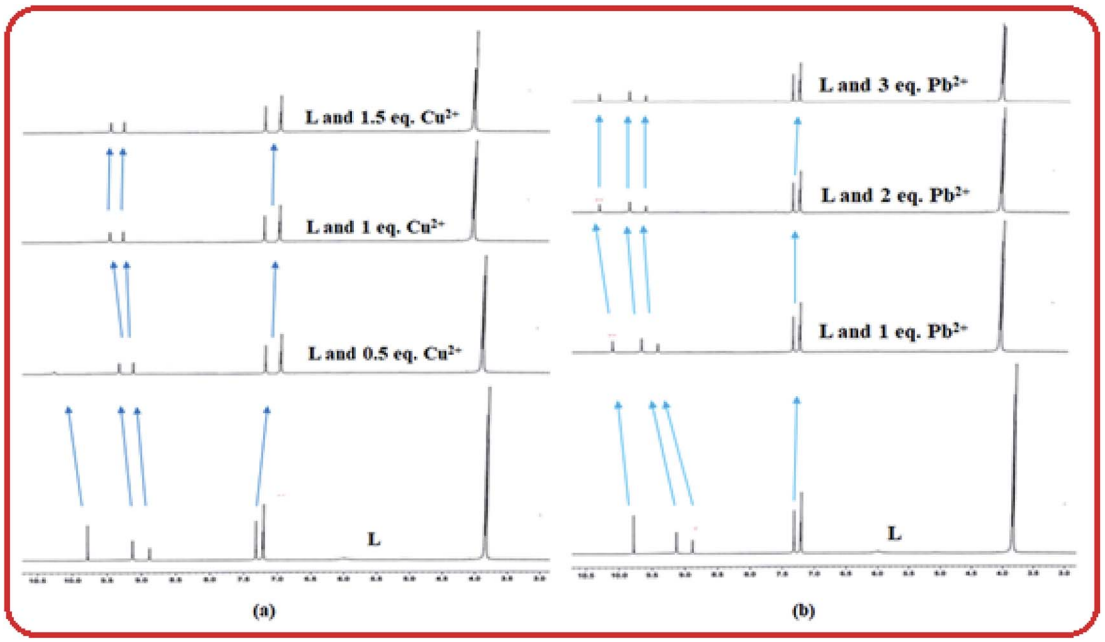

Fig. 9 ^{1}H-NMR titration of L in presence of (a) Cu^{2+} and (b) Pb^{2+}.

measurements and IR-spectral analysis it is evident that the complex **1** is Cu(I) while complex **2** is a Pb(II) complex. Solvent methanol here may be acting as the reducing agent for the reduction of Cu(II) to Cu(I).

Herein, the metal sensing is primarily due to analytes recognition to binding site and signal transduction mechanism. The imine attached triazole moiety contains multiple pockets suitable for metal coordination whereas the phenol containing two methoxy group acts as a signalling sub-unit. Starting from absorption spectra, strong red shift absorption gives an indication for complexation at the acceptor site which enhance ICT process in the ground state, causes colorimetric sensing and in the excited both the PET and ICT effect were responsible for fluorometric sensing. As soon as Cu(II) is added to the chemosensor **L**, initially supramolecular host–guest interaction takes place and then it may be reduced to Cu(I). That has also been reflected from the same color and properties of the isolated copper complex from both Cu(II) and Cu(I) salt. In case of Pb^{2+} recognition, only receptor analyte binding takes place which was responsible for optical change. It is worthy to be mentioned here that in the similar condition the probe does not sense Cu(I) ion.[29]

Moreover the fluorescence spectra of **L**–Cu^{2+} complex, some blue shift observed probably due to deprotonation of triazole 'NH' which also behave as donor site in the excited state. Although there were another coordinating sites (–OH and –OMe) but no binding occurs in these regions, confirmed by UV-vis spectra and ^{1}H-NMR studies. The binding mechanism has been shown in Scheme 2.

DFT studies on the metal complexes

In order to get the close approach towards the probable binding mechanism density functional theory (DFT) calculations of the respective complexes were performed. The geometry optimized structures and a schematic representation of the energy of MOs and contours of selected HOMO and LUMO orbitals of both **L**–

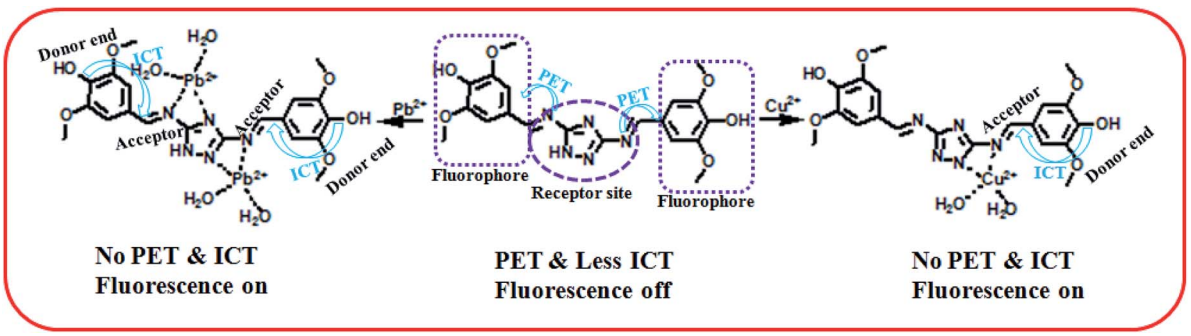

Scheme 2 Proposed sensing mechanism of L.

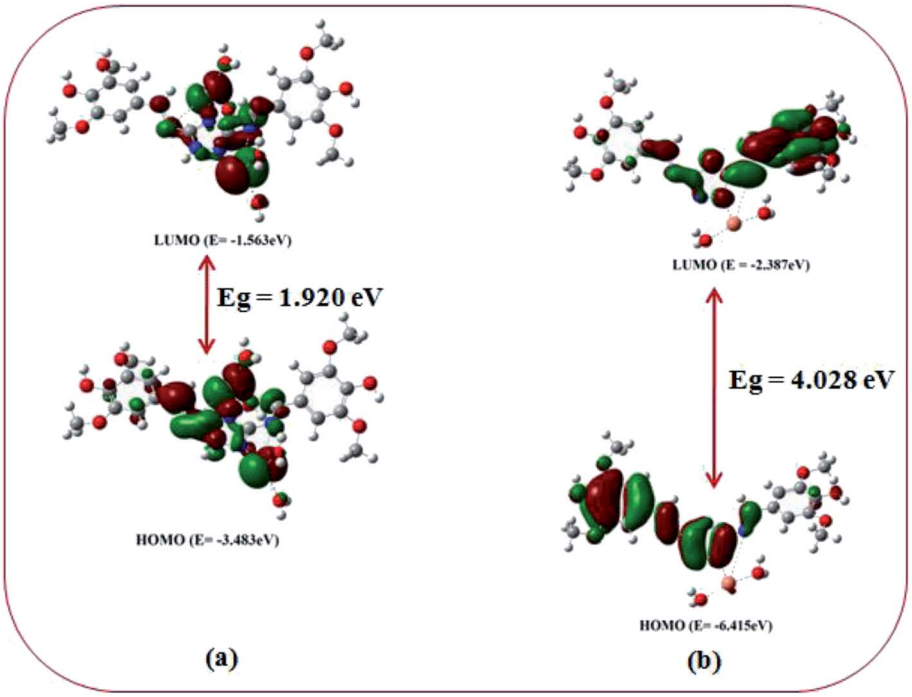

Fig. 10 Frontier molecular orbitals and HOMO–LUMO energy gaps of (a) **L**–Pb^{2+} and (b) **L**–Cu^{2+} complex.

Cu^{2+} and **L**–Pb^{2+} complexes have been shown in Fig. S17† and 10. Notably, the calculated energy gaps between HOMO and LUMO decreased from **L** (5.784 eV) to its M^{2+} complexes (for M = Cu, 4.028 eV; and M = Pb, 1.920 eV). Such lowering of the HOMO–LUMO energy gaps of the chemosensor **L** upon Cu^{2+} and Pb^{2+} complexation attributed to the electron redistributions which resulted in the change in absorbance and fluorescence spectra.

The probe **L** displays a simple approach for the selective detection of Cu^{2+} and Pb^{2+} with enhancement of fluorescence along with red shifted in case of Cu^{2+} and no shift in case of Pb^{2+}. These are because of the restriction of PET (Photoinduced Electron Transfer) as well as ICT (internal

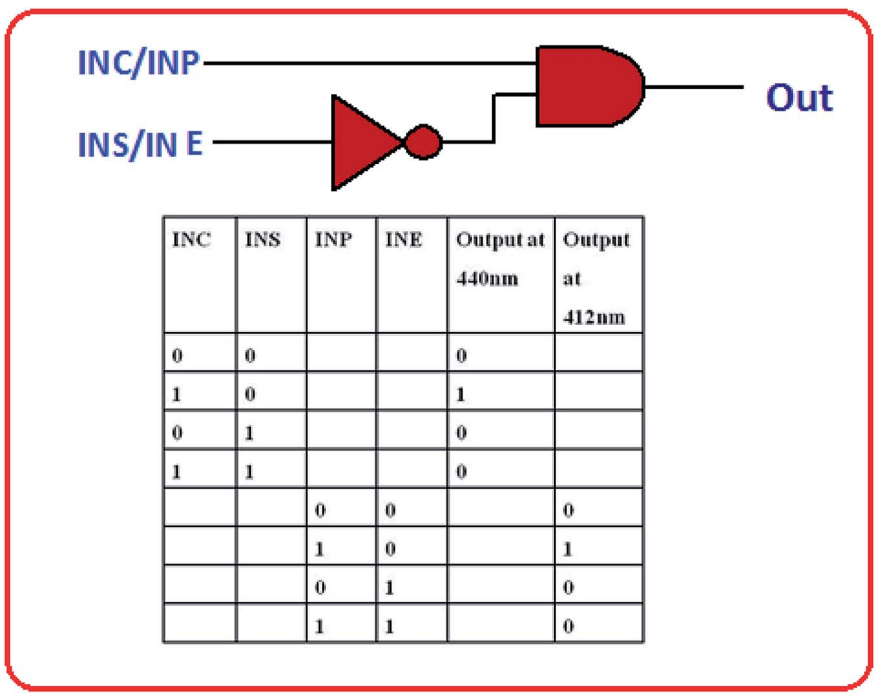

INC	INS	INP	INE	Output at 440nm	Output at 412nm
0	0			0	
1	0			1	
0	1			0	
1	1			0	
		0	0		0
		1	0		1
		0	1		0
		1	1		0

Fig. 11 Truth table and logic scheme for the proposed INHIBIT type logic gate.

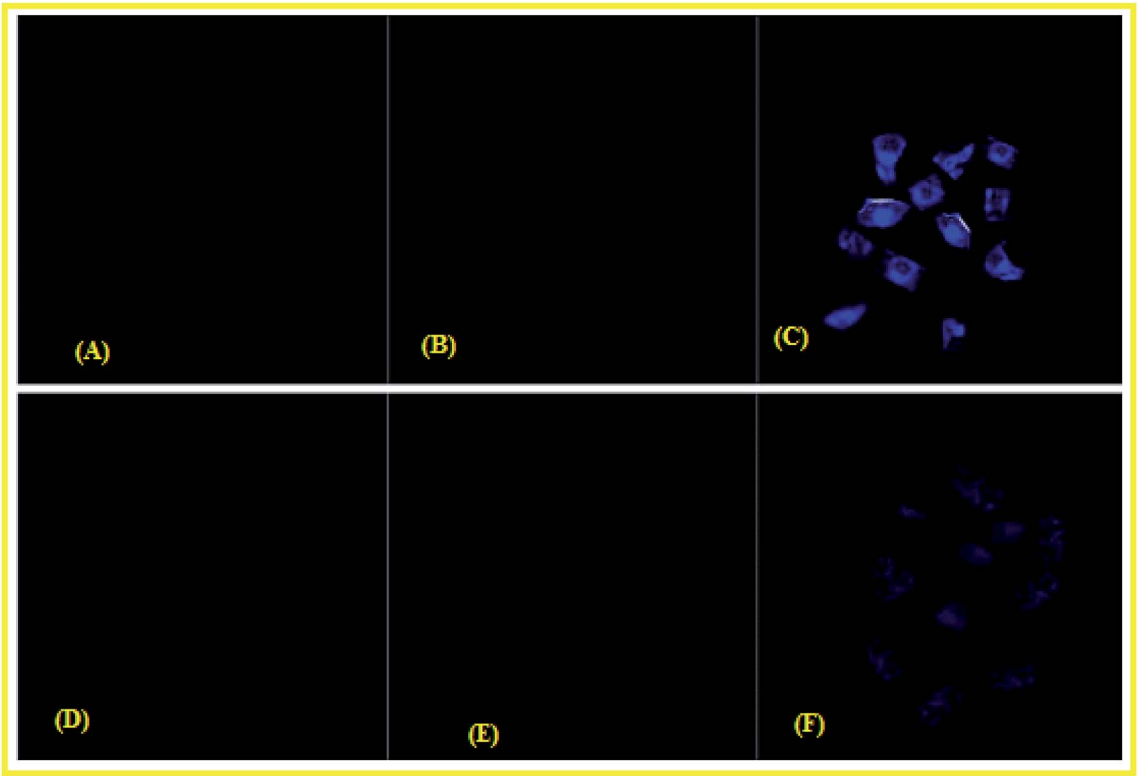

Fig. 12 Fluorescence microscopy images of the HeLa cells after incubation for 2 h (A) cells + probe L (10 μM); (B) cells + Cu^{2+} (10 μM); (C) cells + probe L (10 μM) + Cu^{2+} (10 μM); (D) cells + probe L (10 μM); (E) cells + Pb^{2+} (10 μM); (F) cells + probe L (10 μM) + Pb^{2+} (10 μM).

charge transfer) processes after interaction with Cu^{2+} and Pb^{2+}. From the DFT calculation, it is evident that the easy electronic transition is possible in case of complex **2** in comparison to complex **1**, which also establishes the additional stability of the complex **2**. Specifically, both HOMO and LUMO states of the complexes **1** and **2** in comparing to **L** revealed that the electrons are more delocalized in the complexes **1** and **2**, than in **L** and also in agreement with the barrier of photo-induced electron transfer process, which may results in the enhancement of fluorescence.

Application of the chemosensor L

In building logic gate. Logic gate is a simple and multi-purpose assembly for constructing complicated circuits.[30,31] High emission intensity values are considered as ON state (1) and low intensity values below the threshold value (20 a.u.) are considered as OFF state (0). Considering the fluorescence output signals INHIBT (INH) logic gates were constructed utilizing four ionic inputs. When Cu^{2+} induced to the system, the emission band of **L** at 440 nm, acting as fluorescence ON behaviour. In the next step, the introduction of S^{2-} regenerates the original band of **L** showing OFF behaviour. Again the INHIBIT logic gate was achieved by employing EDTA and Pb^{2+} as two chemical inputs InP and InE respectively. When both the inputs (Pb^{2+} and EDTA) are absent, the output at 412 nm is low indicating OFF state of the system. When InP is present, emission intensity of **L** gets enhanced beyond the threshold value at 412 nm indicating ON state of the system. On the other hand, when only InE is present the emission of **L** is low at this output indicating OFF state again. When both the inputs are present, again displaying the OFF state of the

Table 1 Determination of Pb^{2+} and Cu^{2+} ions in different water samples

Metal ions	Spiked amount (μM)	Recovered amount (μM)	% Recovery ± D ($n = 3$)
Cu^{2+}	5	5.12	101.6 ± 0.2
	10	9.89	99.4 ± 0.83
	20	19.98	98.3 ± 1.32
Pb^{2+}	5	5.09	101.4 ± 0.97
	10	10.95	109.8 ± 0.8
	20	20.02	100.7 ± 1.8

Table 2 Comparison of some previously reported chemosensors for Cu^{2+} and Pb^{2+} ions

Structure of probe	Solvent	Sensing method	Binding constant	LOD	Ref.
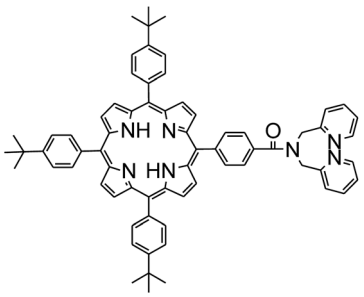	CH_2Cl_2–MeOH (1 : 1)	Both colorimetric and fluorescent	2.1×10^4 for Pb^{2+} and 7.4×10^5 for Cu^{2+}	3.1×10^{-7} M for Pb^{2+} and data not available for Cu^{2+}	32
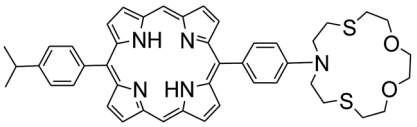	CH_2Cl_2–MeOH (3 : 2)	Both chromogenic and fluorogenic	1.5×10^5 for Cu^{2+} and 3.4×10^4 for Pb^{2+}	2.6×10^{-13} M for Cu^{2+} and 1.3×10^{-11} M for Pb^{2+}	33
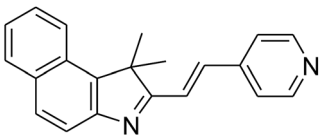	CH_3CN–water mixture (9 : 1, v/v)	Fluorescent sensor	Not available	1.24 μM for Cu^{2+} and 3.41 μM for Pb^{2+}	34
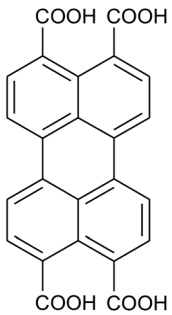	Aqueous solution	Both colorimetric and fluorescent	Not available	Not available	35
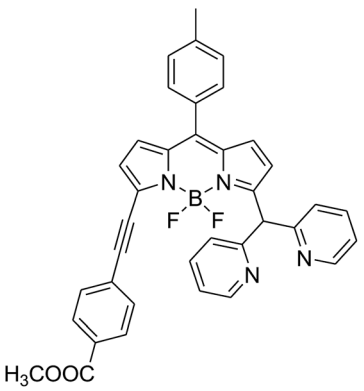	CH_3CN	Colorimetric and fluorescent chemosensor	5.01×10^5 for Pb^{2+} and 8.86×10^5 M^{-1} for Cu^{2+}	0.14 for Pb^{2+} and 0.27 μM for Cu^{2+}	36
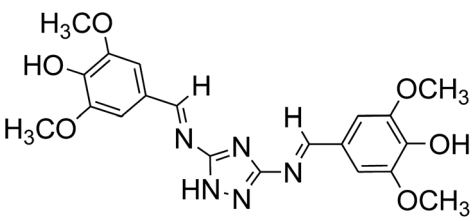	CH_3OH–tris buffer (1 : 1, v/v)	Colorimetric and fluorescent chemosensor	4.7×10^4 M^{-1} for Cu^{2+} and 1.43×10^{11} M^{-2} for Pb^{2+}	12×10^{-7} M^{-1} for Cu^{2+} and 9×10^{-7} M^{-1} for Pb^{2+}	Present work

system. Thus, these combinations lead to construction of INHIBIT logic gate. The logical behaviour and the corresponding truth table are shown in Fig. 11.

Cell imaging studies. To validate the capability of **L** for detecting Cu^{2+} and Pb^{2+} in living cells, bio-imaging experiments were carried out. HeLa cells were first incubated with 10 μM **L**

for 2 h, and then treated with 50 μM $Cu(NO_3)_2$ for 2 h. No fluorescence was observed when cells were exposed to the **L** as shown in Fig. 12(A); but strong fluorescence was observed by the incubation of Cu^{2+} within the cells. Similarly after treatment with Pb^{2+}, a large enhancement in fluorescence was observed. Such results pointed that he complex **L** is cell-permeable and can be used to image intracellular Cu^{2+} and Pb^{2+} ions within living cells [Fig. 12(C) and (F)].

Analysis of biological samples. In order to check the potentiality of the chemosensor **L** in biological samples, the probe **L** of conc. 10 μM, was successfully exploited for the recognition of Pb^{2+} and Cu^{2+} in aqueous solution of bovine serum albumin (BSA) protein by fluorometry. Upon successive addition of Pb^{2+} and Cu^{2+}, the fluorescence intensity was increased in bovine serum albumin (BSA) medium. Almost 21 fold enhancement in emission intensity was observed in case of Pb^{2+}. Cu^{2+} displayed 17 fold rise, pointed that fluorescence emission occurs due to **L**–M^{2+} complexation (M = Pb and Cu) in BSA medium (Fig. S18†).

Real sample analysis. The chemosensor **L** has been utilized successfully in the recognition of both Cu^{2+} and Pb^{2+} ions in different water samples. Hence for this purpose Pb^{2+} and Cu^{2+} ions contaminated samples have been prepared individually through spiking different known concentration levels. Then their concentrations will be analysed with the above sensing system. The experiment was repeated 3 times and good recovery with very less standard deviation was observed. The results have been presented in Table 1.

Comparison of L with other previously reported dual chemosensors for Cu^{2+} and Pb^{2+} ions. As part of our ongoing effort for providing useful analytical techniques to monitor the increasing number of analytes of environmental relevance as quickly and as cheaply as possible and with the highest order of sensitivity, the present paper describes the synthesis of a new fluorescent-colorimetric probe **L**, which was validated for detection and quantification of Cu^{2+} and Pb^{2+} ions in real samples in methanol–tris-HCl buffer medium.

To the best of our knowledge there is no reported Schiff base which shows colorimetric and fluorometric dual selectivity for Cu^{2+} and Pb^{2+}. However there are several reports where few macrocyclic and bodipy systems have been utilized for the selective detection of Cu^{2+} and Pb^{2+} ions. The probe **L**, was compared with those reported chemosensors (Table 2). While each of the other chemosensors showed some advantages such as high sensitivity and selectivity, the important features of the fluorescent-colorimetric chemosensor, **L** are easy, practical and cost effective synthesis and naked eye detection using both colorimetry and fluorometry.

Conclusions

In conclusion, we reported a simple colorimetric and turn-on fluorescent novel bis Schiff base chemosensor **L** containing triazole moiety for selective and sensitive detection Cu^{2+} and Pb^{2+} in CH_3OH–tris buffer (1 : 1, v/v). **L** showed excellent fluorescent properties with distinct naked eye color changes in presence of Cu^{2+} and Pb^{2+} ions. However there are several reports on fluorescence-enhanced probes for these cations separately, but there is no report about the reversible "OFF–ON" fluorescent probe for Cu^{2+} and Pb^{2+} ions together, based on triazole Schiff base. Additionally, the sensing mechanism was investigated by ^{1}H-NMR, FTIR, ESI-mass spectrometry and DFT studies. The fluorometric detection limits for Cu^{2+} and Pb^{2+} were found to be 12×10^{-7} M and 9×10^{-7} M and the colorimetric detection limits were 3.7×10^{-6} M and 1.2×10^{-6} M respectively; which are far below than the permissible concentration in drinking water determined by WHO. The chemosensor **L** shows its application potential in the detection of Cu^{2+} and Pb^{2+} ions in living cells and building INHIBIT type of molecular logic gate.

Conflicts of interest

The authors declare no conflicts of interest.

Acknowledgements

G. K.·P. would like to thank the Department of Science and Technology (SR/FST/CSI-264/2014) and Department of Biotechnology, Government of India, New Delhi for financial support. One of the authors A. K. M. thanks the CSIR, and KR thanks DST, Government of India (No. PDF/2017/001365) for research fellowships.

References

1 Y. Yang, C.-Y. Gao, N. Zhang and D. Dong, *Sens. Actuators, B*, 2016, **222**, 741.
2 D. Udhayakumaria, S. Velmathia, Y.-M. Sung and S.-P. Wu, *Sens. Actuators, B*, 2014, **198**, 285.
3 B. Sarkar, *Chem. Rev.*, 1999, **99**, 2535.
4 H. J. Jang, T. G. Jo and C. Kim, *RSC Adv.*, 2017, **7**, 17650.
5 A. K. Manna, J. Mondal, R. Chandra, K. Rout and G. K. Patra, *J. Photochem. Photobiol., A*, 2018, **356**, 477.
6 E. Madsen and J. D. Gitlin, *Annu. Rev. Neurosci.*, 2007, **30**, 317.
7 M. G. Choi, S. Cha, H. Lee, H. L. Jeon and S.-K. Chang, *Chem. Commun.*, 2009, 7390.
8 M. H. Lim, B. A. Wong, W. H. Pitcock, D. Mokshagundam, M.-H. Baik and S. J. Lippard, *J. Am. Chem. Soc.*, 2006, **128**, 14364.
9 N. Roy, S. Nath, A. Dutta, P. Mondal, P. C. Paula and T. S. Singh, *RSC Adv.*, 2016, **6**, 63837.
10 L. Wang, Q. Bing, G. Wang and J. Li, *J. Photochem. Photobiol., A*, 2018, **360**, 86.
11 A. Ghorai, J. Mondal, A. K. Manna, S. Chowdhury and G. K. Patra, *Anal. Methods*, 2018, **10**, 1063.
12 A. K. Manna, J. Mondal, K. Rout and G. K. Patra, *J. Photochem. Photobiol., A*, 2018, **367**, 74.
13 A. K. Manna, J. Mondal, K. Rout and G. K. Patra, *Sens. Actuators, B*, 2018, **275**, 350.
14 B. N. Ahamed, I. Ravikumar and P. Ghosh, *New J. Chem.*, 2009, **33**, 1825.
15 L. N. Neupane, J.-Y. Park, J. H. Park and K.-H. Lee, *Org. Lett.*, 2013, **15**, 254.

16 O. Sunnapu, N. G. Kotla, B. Maddiboyina, S. Singaravadivel and G. Sivaraman, *RSC Adv.*, 2016, **6**, 656.
17 A. Ghorai, J. Mondal, R. Saha, S. Bhattacharya and G. K. Patra, *Anal. Methods*, 2016, **8**, 2032.
18 J. Fawell, *Guidelines for Drinking Water Quality*, World Health Organization, Geneva, 2nd edn, 1996, vol. 2, p. 940.
19 L. Zhao, D. Suiand and Y. Wang, *RSC Adv.*, 2015, **5**, 16611.
20 M. Zhao, X. Zhou, J. Tang, Z. Deng, X. Xu, Z. Chen, X. Li, L. Yang and L.-J. Ma, *Spectrochim. Acta, Part A*, 2017, **173**, 235.
21 R. Chandra, A. K. Manna, K. Rout, J. Mondal and G. K. Patra, *RSC Adv.*, 2018, **8**, 35946.
22 J. Mondal, A. K. Manna, K. Rout, S. K. Singh, J. P. Naskar and G. K. Patra, *Int. J. Environ. Anal. Chem.*, 2018, **98**, 1160.
23 Y. R. Bhorge, H.-T. Tsai, K.-F. Huang, A. J. Pape, S. N. Janaki and Y.-P. Yen, *Spectrochim. Acta, Part A*, 2014, **130**, 7.
24 A. D. Becke, *J. Chem. Phys.*, 1993, **98**, 5648.
25 C. Lee, W. Yang and R. G. Parr, *Phys. Rev. [Sect.] B*, 1988, **37**, 785.
26 J.-T. Yeh, W.-C. Chen, S.-R. Liu and S.-P. Wu, *New J. Chem.*, 2014, **38**, 4434.
27 L. Tang, M. Cai, Z. Huang, K. Zhong, S. Hou, Y. Bian and R. Nandhakumar, *Sens. Actuators, B*, 2013, **185**, 188.
28 H. A. Benesi and J. H. Hildebrand, *J. Am. Chem. Soc.*, 1949, **71**, 2703.
29 S. Banthia and A. Samanta, *Inorg. Chem.*, 2004, **43**, 6890.
30 A. P de Silva and S. Uchiyama, *Nat. Nanotechnol.*, 2007, **2**, 399.
31 A. P. de Silva and N. D. McClenaghan, *Chem.–Eur. J.*, 2004, **10**, 57.
32 Y. Chen and J. Jiang, *Org. Biomol. Chem.*, 2012, **10**, 4782.
33 Y. Chen and K. Wang, *Photochem. Photobiol. Sci.*, 2013, **12**, 2001.
34 X. Yang, W. Zeng, L. Wang, X. Lu, Y. Yan, J. Qu and R. Liu, *RSC Adv.*, 2014, **4**, 22613.
35 S. Sowmiyha, V. Kumar, J. Pitchaimani, V. Madhu, R. Thiagarajan, N. S. Subramanian and S. P. Anthony, *J. Lumin.*, 2018, **203**, 42.
36 Z. Gu, H. Cheng, X. Shen, T. He, K. Jiang, H. Qiu, Q. Zhang and S. Yin, *Spectrochim. Acta, Part A*, 2018, **203**, 315.